Nucleic Acids Research, 2025, **53**, gkaf040
https://doi.org/10.1093/nar/gkaf040
Advance access publication date: 30 January 2025
Chemical Biology and Nucleic Acid Chemistry

Direct repeat region 3′ end modifications regulate Cas12a activity and expand its applications

Wei Zhang[1,†], Yinyin Zhong[1,†], Jiaqi Wang[1,†], Guangrong Zou[2], Qiaozhen Chen[3], Chaoxing Liu[1,*]

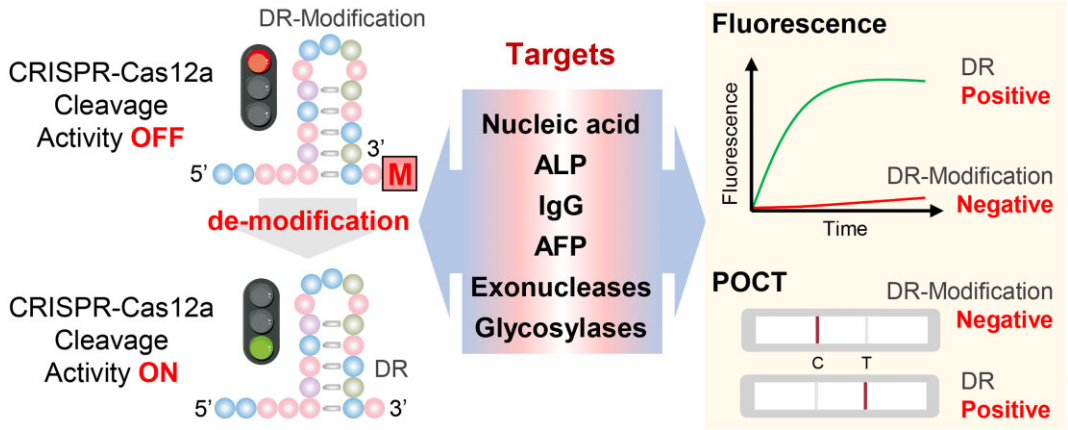
[1]Guangdong Provincial Key Laboratory of Digestive Cancer Research, Digestive Diseases Center, Scientific Research Center, The Seventh Affiliated Hospital of Sun Yat-sen University, Shenzhen, Guangdong 518107, P.R. China
[2]Department of Clinical Laboratory, The Seventh Affiliated Hospital of Sun Yat-sen University, Shenzhen, Guangdong 518107, P.R. China
[3]School of Chemistry and Biological Engineering, University of Science and Technology Beijing, Beijing 100083, P.R. China

[*]To whom correspondence should be addressed. Email: liuchx69@mail.sysu.edu.cn
[†]The first three authors should be regarded as Joint First Authors.

Abstract

CRISPR-Cas12a technology has transformative potential, but as its applications grow, enhancing its inherent functionalities is essential to meet diverse demands. Here, we reveal a regulatory mechanism for LbCas12a through direct repeat (DR) region 3′ end modifications and de-modifications, which can regulate LbCas12a's *cis*- and *trans*-cleavage activities. We extensively explored the effects of introducing phosphorylation, DNA, photo-cleavable linker, DNA modifications at the DR 3′ end on LbCas12a's functionality. We find that the temporary inhibitory function of Cas12a can be reactivated by DR 3′ end modification corresponding substances, such as alkaline phosphatase (ALP), immunoglobulin G (IgG), alpha-fetoprotein (AFP), DNA exonucleases, ultraviolet radiation, and DNA glycosylases, which greatly expand the scope of application of Cas12a. Clinical applications demonstrated promising results in ALP, AFP, and trace Epstein–Barr virus detection compared to gold standard methods. Our research provides valuable insights into regulating LbCas12a activity through direct modification of DR and significantly expands its potential clinical detection targets, paving the way for future universal clustered regularly interspaced short palindromic repeats (CRISPR) diagnostic strategies.

Graphical abstract



Introduction

Since its inception, clustered regularly interspaced short palindromic repeats (CRISPR) technology has revolutionized the fields of molecular biology and biomedicine [1]. Originally derived from bacterial immune systems that protect against foreign genetic invasions, CRISPR has evolved into a versatile tool for gene editing and *in vitro* diagnostics [2]. The technology is based on two fundamental components: CRISPR RNA (crRNA) and CRISPR-associated proteins (Cas proteins) [3]. Here, crRNA identifies specific nucleic acid sequences, while Cas proteins perform nucleic acid cleavage, encompassing both *cis*- and *trans*-cleavage mechanisms [4–6]. This straightforward yet effective system enables precise nucleic acid recognition, providing a robust foundation for applications in gene editing, cellular imaging, transcriptional regulation, and molecular diagnostics [1, 7–9].

Despite its transformative impact, the expanding applications of CRISPR technology necessitate enhancements to its

Received: December 2, 2024. **Revised:** January 13, 2025. **Editorial Decision:** January 14, 2025. **Accepted:** January 16, 2025
© The Author(s) 2025. Published by Oxford University Press on behalf of Nucleic Acids Research.
This is an Open Access article distributed under the terms of the Creative Commons Attribution-NonCommercial License (https://creativecommons.org/licenses/by-nc/4.0/), which permits non-commercial re-use, distribution, and reproduction in any medium, provided the original work is properly cited. For commercial re-use, please contact reprints@oup.com for reprints and translation rights for reprints. All other permissions can be obtained through our RightsLink service via the Permissions link on the article page on our site—for further information please contact journals.permissions@oup.com.

Downloaded from https://academic.oup.com/nar/article/53/3/gkaf040/7990341 by guest on 10 February 2025

inherent capabilities to meet diverse and growing demands [1–3]. A comprehensive investigation of the intricate details and sophisticated regulatory mechanisms of CRISPR components has the potential to enhance the precision, sensitivity, and programmability of this technology [10, 11]. Notably, the identification and expression of more Cas proteins from various strains and the engineered modification of these proteins can introduce specialized features, including light control [12–14], heat resistance [15], high selectivity [16, 17], and single-base resolution recognition of targets [18]. In addition, modifications to crRNA—such as elongation [19, 20], shortening [21, 22], splitting [23–25], introducing secondary structures [26, 27], embedding in DNA [20, 21], substituting conventional bases with naturally occurring [28–30] or synthetic nucleic acid modifications [31–33], and incorporating complementary sequences [34–39]—offer promising avenues for accurate regulation of Cas protein activity.

Specifically, in the CRISPR-Cas12a nucleic acid detection system, optimizing the DNA reporter and implementing novel structures like hairpin [40], DNA Framework [41], and nanoparticles [42, 43] can significantly enhance *trans*-cleavage capabilities for effective signal amplification. Furthermore, adaptations to the substrate DNA activator for Cas12a—including blocking [44], circularization [45], and splitting techniques [25, 46, 47]—enable the detection of non-nucleic acid targets [44], facilitate signal amplification [45], and microRNA (miRNA) detection [25, 47]. Additionally, optimizing magnesium ion concentrations [48] and introducing physical barriers in the reaction system [49] are pivotal for improving regulatory outcomes.

While these advancements have broadened the application spectrum of CRISPR, they also underscore the urgent need for ongoing development and highlight the limitations of current methodologies, particularly the extensive experimental optimizations often required across diverse application contexts [1, 11]. As CRISPR technology continues to evolve, the challenge remains to achieve precise control over Cas proteins without compromising efficiency [1, 3]. Although existing methods to modulate Cas protein activity have made significant strides, there is an urgent requirement for more generalized, flexible, and efficient control strategies tailored to specific applications across various fields, thereby expanding the current utilization landscape [11].

Recent discoveries indicate that the Cas12a' crRNA can be divided into a universal direct repeat (DR) region and a replaceable spacer region, which can still maintain the Cas12a *cis*- and *trans*-cleavage activity [23–25]. This enables the design of universal strategies targeting the DR, applicable to an array of nucleic acid detection targets while facilitating nucleic acid cascade signal amplification and miRNA detection [23–25]. An in-depth investigation of this universal DR has the potential to enhance the adaptability of CRISPR methodologies and tackle existing technological limitations, thereby opening new pathways for future biomedical research.

In this study, we demonstrate that modifications at the 3′ end of the DR can effectively suppress Cas12a activity, with subsequent removal of these modifications restoring its functionality. We conduct a systematic investigation of various modifications at this site, including phosphorylation, addition of DNA, photo-cleavable (PC) linker, and DNA modifications (Supplementary Scheme S1), elucidating the mechanisms behind the inhibition and restoration of Cas12a activity (Fig. 1). Our findings have been applied to the rapid and highly sensitive detection of clinical analytes, including alkaline phosphatase (ALP), alpha-fetoprotein (AFP), and Epstein-Barr virus (EBV) in human serum, as well as various DNA glycosylases corresponding to specific DNA modifications. This work not only advances our understanding of universal Cas12a regulation but also explores programmable detection principles for non-nucleic acid targets beyond aptamers, thereby significantly broadening its clinical applicability.

Materials and methods

Ethics statement

Human blood samples were collected and provided by the Seventh Affiliated Hospital, Sun Yat-sen University with protocols approved by the ethics committee at the Seventh Affiliated Hospital, Sun Yat-sen University (KY-2024-303-02, KY-2023-117-01, KY-2024-100-01, and KY-2024-009-02). All patients in this study signed an informed consent form.

Agarose gel analysis of LbCas12a's *Cis*-cleavage activity regulated by different DR 3′ modifications

ALP-DR-3′PO_4 Regulation: The reaction was prepared at a final concentration of 1 × LbCas12a Reaction Buffer, comprising 10 mM Tris–HCl (pH 8.5), 10 mM $MgCl_2$, 20 mM KCl, 1 mM DTT, 40 mM Glycine, and 0.01% (v/v) Tween 20. To the reaction, 800 nM of either DR-3′PO_4 or DR was added, with or without one unit of ALP. The total volume was adjusted to 10 μl with DNase/RNase-Free distilled water and incubated at 37°C for 30 min. Subsequently, the reaction was supplemented with 1 × LbCas12a Reaction Buffer, 800 nM LbCas12a, 800 nM of various Spacers [EBV Spacer, hepatitis C virus (HCV) Spacer or monkeypox virus (MPXV) Spacer], and 30 nM of their respective targets. The total volume was brought to 20 μl and incubated at 37°C for an additional 30 min. To terminate the reaction, 50 mM Proteinase K was added, followed by incubation at 37°C for 20 min. Finally, 1 × loading buffer was added, and the samples were subjected to 2% agarose gel electrophoresis.

Exonuclease I (Exo I)-DR-DNA Regulation: The reaction was prepared at a final concentration of 1 × LbCas12a Reaction Buffer and included 1 μM of either DR-DNA or DR, with or without two units of Exo I. The total volume was adjusted to 10 μl with DNase/RNase-Free distilled water and incubated at 37°C for 1 h, followed by heat inactivation at 65°C for 10 min. Next, 1 × LbCas12a Reaction Buffer was added, along with 300 nM LbCas12a, 1 μM of various Spacers (EBV Spacer, HCV Spacer or MPXV Spacer), and 30 nM of their respective targets. The total volume was again adjusted to 20 μl and incubated at 37°C for 1 h. To terminate the reaction, 50 mM Proteinase K was added, and the incubation continued at 37°C for 20 min. Afterward, 1 × loading buffer was included, and the samples were analyzed using 2% agarose gel electrophoresis.

UV Light-DR-PC-DNA Regulation: The reaction was conducted using 1 × LbCas12a Reaction Buffer with five units of T4 Polynucleotide Kinase, 0.5 mM adenosine diphosphate (ADP), 1 μM of either DR-PC-DNA or DR, 500 nM LbCas12a, 1 μM MPXV Spacer, and 5 nM MPXV target. The total volume was adjusted to 20 μl, with or without exposure to UV light (λ = 365 nm, 35 W for 15 s). The mixture was then incubated at 37°C for 1 h. To terminate the reaction, 50 mM Proteinase K was added and incubated at 37°C

Downloaded from https://academic.oup.com/nar/article/53/3/gkaf040/7990341 by guest on 10 February 2025

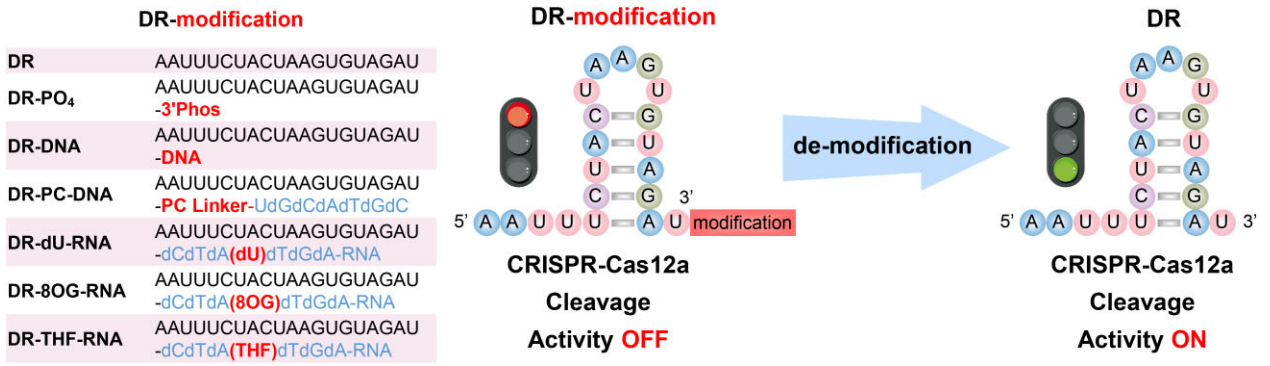


Figure 1. Schematic representation of the DR and its 3′ end modifications, illustrating their regulatory effects on LbCas12a protein activity.

for an additional 20 min. Finally, 1 × loading buffer was incorporated, and the samples were examined via 2% agarose gel electrophoresis.

Real-time fluorescence quantitative detection analysis of LbCas12a's *Trans*-cleavage activity regulated by different DR 3′ modifications

ALP-DR-3′PO_4 Regulation: the reaction was prepared using 1 × LbCas12a Reaction Buffer with 30 nM of either DR-3′PO_4 or DR, supplemented with one unit of ALP or left untreated. The total volume was adjusted to 10 μl with DNase/RNase-Free distilled water and incubated at 37°C for 30 min. Following this step, 1 × LbCas12a Reaction Buffer, 100 nM LbCas12a, 250 nM F-Q, 30 nM of various Spacers (EBV Spacer, HCV Spacer, or MPXV Spacer), and 2 nM of their respective targets were added to the mixture, bringing the total volume to 20 μl. The reaction was mixed thoroughly in a quantitative PCR (qPCR) tube and promptly placed into the qPCR instrument, where it was incubated at 37°C. Fluorescence was collected every 30 s over a total of 60 cycles for 30 min. Notes: The photosensitive reagent F-Q was stored in an Eppendorf (EP) amber tube protected from light at −20°C to maintain its stability and functionality before use.

Exo I-DR-DNA Regulation: the reaction was conducted in 1 × LbCas12a Reaction Buffer, containing 50 nM of either DR-DNA or DR, with or without two units of Exo I. The volume was adjusted to 10 μl with DNase/RNase-Free distilled water and incubated at 37°C for 1 h, followed by heat inactivation at 65°C for 10 min. Subsequently, 1 × LbCas12a Reaction Buffer, 100 nM LbCas12a, 250 nM F-Q, 50 nM of various Spacers (EBV Spacer, HCV Spacer, or MPXV Spacer), and 3 nM of their respective targets were added, filling the total volume to 20 μl. The mixture was then mixed in a qPCR tube and quickly transferred to the qPCR instrument, maintained at 37°C, collecting fluorescence every 30 s over a span of 60 cycles for 30 min.

UV Light-DR-PC-DNA Regulation: the reaction was set up using 1 × LbCas12a Reaction Buffer, supplemented with five units of T4 Polynucleotide Kinase and 0.5 mM ADP. The reaction included 100 nM of either DR-PC-DNA or DR, along with 100 nM LbCas12a, 250 nM F-Q, 100 nM MPXV Spacer, and 5 nM MPXV target, adjusted to a total volume of 20 μl. Two conditions were established: one exposed to UV light (λ = 365 nm, 35 W for 15 s) and one without UV exposure. The mixture was thoroughly mixed in a qPCR tube and quickly placed into the qPCR instrument, where it was incubated at 37°C. Fluorescence was collected every 30 s for a total of 60 cycles over 30 min.

Michaelis-Menten model for *Trans*-cleavage activity of DR-PO_4 assisted LbCas12a

The reaction was conducted in 1 × LbCas12a Reaction Buffer containing 100 nM DR-3′PO_4 or 100 nM DR, supplemented with or without one unit of ALP and adjusted to a total volume of 10 μl with DNase/RNase-Free distilled water. The mixture was incubated at 37°C for 30 min. Following this incubation, 1 × LbCas12a Reaction Buffer, 50 nM LbCas12a, 100 nM EBV Spacer, and 3 nM EBV target were added, resulting in a total volume of 18 μl, and incubated at 37°C for an additional 15 min. Subsequently, 2 μl of F-Q at varying concentrations (500, 250, 125, 62.5, 31.25, 15.63, and 0 nM) were mixed in, and the reaction was transferred to a qPCR instrument set at 37°C, collecting fluorescence data every 10 s for a total of 180 cycles over 30 min. The data were calculated based on the formula in the previous report paper [50].

Detection of alkaline phosphatase using DR-PO_4 assisted CRISPR-Cas12a system

The reaction was set up with 1 × LbCas12a Reaction Buffer, containing 400 nM DR-3′PO_4. To this, 2 μl of diluted ALP standard (800, 400, 200, 100, 50, 25, 12.5, 6.25, 3.13, or 0 U/L) or the sample for testing was added, and the final volume was adjusted to 10 μl with DNase/RNase-Free distilled water. The mixture was incubated at 37°C for 30 min. Then, 1 × LbCas12a Reaction Buffer, 100 nM LbCas12a, 250 nM F-Q, 30 nM EBV Spacer, and 8 nM EBV target were added, bringing the total volume to 20 μl. The reaction was mixed thoroughly in a qPCR tube and quickly placed into the qPCR instrument at 37°C, where fluorescence measurements were taken every 30 s over a total of 20 cycles for 10 min. The fluorescence value of the sample was then used to calculate the sample concentration by referencing the linear equation generated from the standards.

Classical PNPP method for alkaline phosphatase detection

In a transparent 96-well plate, 2 μl of diluted ALP standard (800, 400, 200, 100, 50, 25, 12.5, 6.25, 3.13, or 0 U/L) or the test sample was added. Distilled water was added to achieve a final volume of 50 μl, followed by the addition of 50 μl of *p*-nitrophenylphosphate (PNPP) substrate solution (5 mmol/l). The mixture was incubated at 37°C for 20 min, after which 50 μl of PNPP stop solution was added. The optical densities at OD 405 and OD 630 nm were measured using a microplate

Downloaded from https://academic.oup.com/nar/article/53/3/gkaf040/7990341 by guest on 10 February 2025

reader, generating a standard curve. The OD 405–OD 630 nm value of the test sample was then compared to the standard curve to determine the sample concentration.

Detection of mouse IgG using DR-PO_4 assisted CRISPR-Cas12a system

In a 96-well plate, 100 μl of Protein G diluted to 5 μg/ml in PBS was added to each well and sealed. The plate was incubated at 4°C for 14 h. The wells were washed three times with PBST (PBS + 0.05% Tween 20) using 200 μl per wash and then dried. Blocking buffer (200 μl containing 3% BSA in PBS) was added, and the plate was incubated at 37°C for 1 h. After blocking, the wells were washed five times with PBST and dried again. Different concentrations of mouse IgG standards (2500, 1250, 625, 312.5, 156.3, 78.1, 39.1, 19.6, and 0 ng/ml) or unknown samples were diluted to 200 μl and incubated at 37°C for 1 h. Following this incubation, the wells were washed five times with PBST and dried. Then, 100 μl of 1:500 diluted ALP-labeled Goat Anti-Mouse IgG (H + L) was added, followed by another 1 h incubation at 37°C and subsequent washing five times with PBST. Finally, 1 × LbCas12a Reaction Buffer containing 200 nM DR-3′PO_4 was added and adjusted to a total volume of 40 μl with DNase/RNase-Free distilled water. This mixture was incubated at 37°C for 15 min, followed by the addition of 1 × LbCas12a Reaction Buffer, 200 nM LbCas12a, 250 nM F-Q, 200 nM EBV Spacer, and 10 nM EBV target, bringing the final volume to 50 μl. Fluorescence was measured in the FAM channel of a microplate reader every 2 min for 16 min, to determine concentration based on fluorescence values.

Visualization of mouse IgG detection using DR-PO_4 assisted CRISPR-Cas12a lateral flow test strips

The preparatory steps for this assay were consistent with those described in section 5. And the procedure CRISPR assay was modified as follows: 1 × LbCas12a Reaction Buffer containing 200 nM DR-3′PO_4 was added, with the total volume adjusted to 40 μl using DNase/RNase-Free distilled water. This mixture was incubated at 37°C for 20 min. Subsequently, 1 × LbCas12a Reaction Buffer, 200 nM LbCas12a, 250 nM FAM-Biotin DNA reporter, 200 nM EBV Spacer, and 30 nM EBV target were added, adjusting the total volume to 50 μl. The mixture was incubated at 37°C for 1 h before being inserted into the lateral flow test strip (CRISPR) and results were observed after 5 min.

Classical PNPP method for mouse IgG detection

The preparatory steps were consistent with those outlined in section 6. Modifications to the last step included adding 50 μl of PNPP substrate solution (5 mmol/l) to a 96-well plate. Incubation was carried out at 37°C for 20 min, after which 50 μl of PNPP stop solution was added. The optical densities at OD 405 and OD 630 nm were measured to assess the presence of mouse IgG.

Detection of serum AFP using DR-PO_4 assisted CRISPR-Cas12a system

The assay was performed using a purchased microplate pre-coated with human AFP-specific antibodies (Cat No. ELK1301, ELK Biotechnology Co., Ltd., Wuhan, China). Following the manufacturer's instructions, the standards or samples were added to the wells of the microplate, followed by the addition of biotin-conjugated antibodies specific to human AFP. Subsequently, ALP-conjugated Streptavidin (Cat No. 35106ES60, Yeasen Biotechnology Co., Ltd., Shanghai, China) was added to each well and incubated. After incubation, 1 × LbCas12a Reaction Buffer, 200 nM DR-3′PO_4 was added, and the total volume was adjusted to 40 μl with enzyme-free water. The reaction was conducted at 37°C for 15 min. Following this, 1 × LbCas12a Reaction Buffer, 200 nM LbCas12a, 250 nM F-Q, 200 nM EBV Spacer, and 10 nM EBV target were added to achieve a final volume of 50 μl. Fluorescence was measured in the FAM channel of a microplate reader every 2 min for 16 min. The fluorescence data from the samples were compared to the standard curve to calculate the concentration.

Detection of exonuclease I using DR-DNA assisted CRISPR-Cas12a system

The assay was prepared in 1 × LbCas12a Reaction Buffer containing 50 nM DR-DNA. To this, 2 μl of diluted Exo I at varying concentrations (250, 62.5, 15.6, 3.9, 0.98, 0.49, 0.24, 0.12, 0.06, and 0 U/ml) or unknown samples were added, and the total volume was adjusted to 10 μl with enzyme-free water. The reaction was incubated at 37°C for 1 h, followed by inactivation at 65°C for 10 min. Then, 1 × LbCas12a Reaction Buffer, 100 nM LbCas12a, 250 nM F-Q, 50 nM EBV Spacer, and 5 nM EBV target were added, bringing the final volume to 20 μl. The mixture was mixed well and quickly placed into a qPCR tube before being transferred to a qPCR instrument at 37°C, where fluorescence was collected every 30 s, totaling 120 cycles over 60 min.

One-pot RPA-CRISPR-Cas12a nucleic acid detection using DR-PC-DNA

The reaction was conducted in 1 × RPA-CRISPR Reaction Buffer (2 mM Tris–HCl, pH 8.5, 28 mM $MgCl_2$, 4 mM KCl, 0.2 mM DTT, 8 mM glycine, 0.002% (v/v) Tween 20, 0.5 mM ADP), with the addition of 10 units of T4 Polynucleotide kinase, 100 nM LbCas12a, 100 nM DR-PC-DNA, 100 nM EBV Spacer, and 250 nM F-Q. A total volume of 20 μl was achieved by adding 9 μl of RT-RPA 2.0 Mix, 0.1 μM EB-RPA-F, 0.1 μM EB-RPA-R, and varying concentrations of EBV target (50, 5, 0.5, 0.05, and 0 copies/μl) or unknown samples. All reagents were mixed and placed in a qPCR tube, then transferred to the qPCR instrument at 37°C for RPA amplification. Fluorescence was collected every 5 min for a total of three cycles over 15 min. Post-amplification, the qPCR tube was exposed to UV light ($\lambda = 365$ nm, 35 W) for 15 s before being returned to the qPCR instrument for another 45 min of fluorescence collection every 30 s, totaling 90 cycles. The concentration of the unknown samples was calculated by referencing the standard curve. Notes: The photosensitive DR-PC-DNA was aliquoted and stored in light-protected EP tubes at −80°C to prevent any potential photodegradation before use.

RT-qPCR assessment of clinical EBV samples

The assay utilized Hieff® 1 × qPCR SYBR Green Master Mix (No Rox), with 0.1 μM EB-RPA-F, 0.1 μM EB-RPA-R, and 2 μl of standards or samples at varying concentrations. The total volume was adjusted to 20 μl with enzyme-free water and mixed well before being placed in the qPCR instrument. The cycling parameters included an initial denaturation at 95°C for 3 min, followed by 40 cycles of denaturation at 95°C for

Downloaded from https://academic.oup.com/nar/article/53/3/gkaf040/7990341 by guest on 10 February 2025

10 s and annealing/extension at 55°C for 30 s, with fluorescence detection at each cycle. The Ct values obtained from the standards were used to quantify the concentration of the clinical samples.

Detection of UDG content using DR-dU-RNA assisted CRISPR-Cas12a and visualization on test strips

The detection was performed in 1 × LbCas12a-UDG Reaction Buffer (10 mM Tris–HCl, pH 8.5, 10 mM $MgCl_2$, 20 mM KCl, 1 mM DTT, 40 mM glycine, 1 mM spermidine, and 0.01% (v/v) Tween 20) containing 80 nM DR-dU-RNA and 10 units of Exo I & III. A volume of 2 μl from various concentrations of UDG standards (500, 250, 125, 62.5, 31.25, 15.63, 7.81, and 0 U/L) or extracted nuclear protein samples (HCT116, SW480 diluted 4-fold, NCM460 diluted 2-fold) was added, followed by adjustment to a total volume of 10 μl with enzyme-free water. The 1 × LbCas12a-UDG Reaction Buffer was consistently utilized as the dilution buffer throughout this study, ensuring that variations in dilution times would not compromise the performance or stability of the reaction system. The reaction was incubated at 37°C for 30 min and then inactivated at 65°C for 10 min. Afterward, 1 × LbCas12a-UDG Reaction Buffer, 100 nM LbCas12a, 250 nM F-Q, 80 nM EBV Spacer, and 8 nM EBV target were added to reach a total volume of 20 μl. The mixture was quickly transferred to a qPCR instrument and incubated at 37°C, where fluorescence was collected every 30 s for 24 cycles totaling 12 min. The UDG content in extracted nuclear proteins from different cell lines was calculated using the standard curve. For test strip detection, F-Q was replaced with FAM-Biotin, and after the reaction, the mixture was introduced into the test strip for detection, with results observed after 5 min.

Detection of OGG1 using DR-8OG-RNA assisted CRISPR-Cas12a

The assay was conducted in 1 × LbCas12a Reaction Buffer containing 80 nM DR-8OG-RNA and 10 units of Exo I & III. A volume of 1 μl from varying concentrations of OGG1 standards (8000, 4000, 2000, 1000, 500, 250, 125, and 0 U/ml) or unknown samples was added, followed by adjustment to a total volume of 10 μl with enzyme-free water. The mixture was incubated at 37°C for 30 min and inactivated at 65°C for 10 min. Subsequently, 1 × LbCas12a Reaction Buffer, 200 nM LbCas12a, 250 nM F-Q, 200 nM EBV Spacer, and 8 nM EBV target were added, bringing the final volume to 20 μl. The mixture was rapidly transferred to a qPCR instrument, and fluorescence was collected every 30 s for a total of 60 cycles over 30 min.

Detection of APE1 content using DR-THF-RNA assisted CRISPR-Cas12a

The reaction was performed in 1 × LbCas12a Reaction Buffer containing 200 nM DR-THF-RNA and four units of Exo I & III. A volume of 1 μl from varying concentrations of APE1 standards (10 000, 5000, 2500, 1250, 625, 312.5, 156.3, and 0 U/ml) or unknown samples was added, and the total volume was adjusted to 10 μl with enzyme-free water. The mixture was incubated at 37°C for 1 h, followed by inactivation at 65°C for 10 min. Afterward, 1 × LbCas12a Reaction Buffer, 200 nM LbCas12a, 250 nM F-Q, 200 nM EBV Spacer, and 8 nM EBV target were added to reach a total volume of 20 μl. The assay was quickly placed into a qPCR instrument at 37°C, with fluorescence recorded every 30 s for a total of 120 cycles over 60 min.

Data processing and analysis

All experimental data are expressed as mean ± standard error of the mean from three independent technical replicates. Statistical analyses were conducted using GraphPad Prism software (version 9.0). *P*-values for the statistical analysis were performed by two-sample unpaired *t*-test to define significant differences for different conditions. For linear regression analysis, data points were systematically selected from fluorescence kinetic curves based on three established criteria: (i) exclusion of plateau-phase data points to ensure analysis within the linear amplification range; (ii) demonstration of statistically significant differences ($P < 0.05$) in fluorescence intensity across the target concentration gradient at the selected time point; and (iii) maintenance of a strong linear correlation ($R^2 > 0.9$) between fluorescence intensity and target concentration. These selection criteria were implemented to ensure robust quantification and minimize potential artifacts in the quantitative analysis.

Results

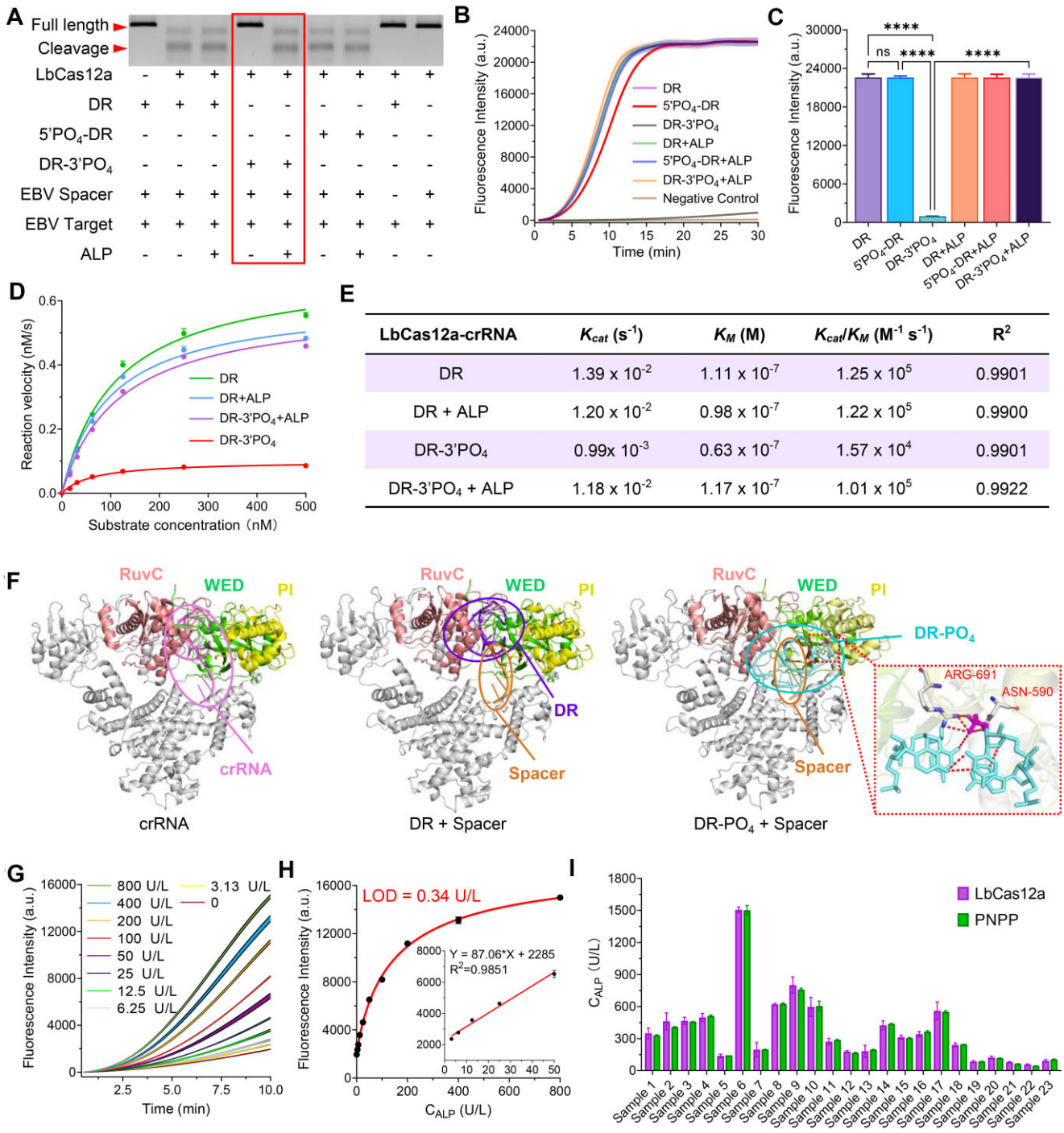
Regulation of LbCas12a activity by phosphorylation at the 3′ end of the DR

Main Initially, we designed and synthesized a classic DR, along with two variations: a 5′ phosphorylated DR (5′PO_4-DR, Supplementary Table S1) and a 3′ phosphorylated DR (DR-3′PO_4, Supplementary Table S1). To evaluate their efficacy, we matched them with an EBV Spacer and used an EBV target for *cis*-cleavage activity assays. As shown in Fig. 2A, both the classic DR and the 5′PO_4-DR demonstrated effective targeting and cleavage of the EBV target, resulting in the formation of cleaved nucleic acid bands. In contrast, the DR-3′PO_4 was unable to mediate cleavage. However, upon the introduction of ALP, which removes 5′ and 3′ phosphate groups, the *cis*-cleavage capacity of DR-3′PO_4 was significantly restored, exhibiting performance comparable to that of the classic DR and 5′PO_4-DR. This experiment confirms that phosphorylation at the 3′ end of the DR profoundly suppresses the *cis*-cleavage activity of LbCas12a (Fig. 2A).

Next, we introduced a single-stranded DNA reporter (F-Q, Supplementary Table S1), labeled with FAM at one end and BHQ1 (a fluorescent quencher) at the other, to assess *trans*-cleavage activity. Activated LbCas12a efficiently *trans*-cleaved the F-Q, leading to the release of a fluorescent signal [4, 5]. As illustrated in Figs 2B and C, DR-3′PO_4 significantly inhibited LbCas12a's *trans*-cleavage activity, but fluorescence was restored upon the addition of ALP. This further validates the role of the 3′ phosphorylation of the DR in modulating LbCas12a activity (Figs 2B and C). We subsequently matched corresponding spacer regions for additional targets, such as HCV and MPXV, confirming the universality of the regulatory effects of the DR 3′ terminal phosphorylation on the system's activity (Supplementary Fig. S1).

We further investigated the impact of DR 3′ phosphorylation on LbCas12a's Michaelis–Menten kinetics [50] (Fig. 2D and E; Supplementary Fig. S2). When the target DNA activated LbCas12a with the classic DR, the catalytic efficiency (K_{cat}/K_M) was measured at 1.25×10^5 M^{-1} S^{-1}. Interestingly, the addition of ALP caused a marginal decrease to

Downloaded from https://academic.oup.com/nar/article/53/3/gkaf040/7990341 by guest on 10 February 2025



LbCas12a-crRNA	K_{cat} (s^{-1})	K_M (M)	K_{cat}/K_M (M^{-1} s^{-1})	R^2
DR	1.39×10^{-2}	1.11×10^{-7}	1.25×10^{5}	0.9901
DR + ALP	1.20×10^{-2}	0.98×10^{-7}	1.22×10^{5}	0.9900
DR-3'PO_4	0.99×10^{-3}	0.63×10^{-7}	1.57×10^{4}	0.9901
DR-3'PO_4 + ALP	1.18×10^{-2}	1.17×10^{-7}	1.01×10^{5}	0.9922

Figure 2. The impact of DR 3′ phosphorylation modification on LbCas12a cleavage activity and its application in clinical ALP detection. (**A**) *Cis*-cleavage activity of LbCas12a assisted by classical DR, terminal phosphorylation-modified DR in conditions with and without ALP. (**B**) Real-time fluorescence detection curves showing LbCas12a's *trans*-cleavage activity with the aforementioned DR, DR modifications in the presence and absence of ALP. (**C**) Quantitative analysis of panel (B). (**D**) Reaction velocity versus substrate concentration curve for the *trans*-cleavage activity of LbCas12a with DR or 3′-phosphorylated DR in the presence and absence of ALP. (**E**) Quantitative data of LbCas12a cleavage activity under different conditions. (**F**) Simulated interaction model between LbCas12a with full length crRNA, split DR and spacer region, and 3′-phosphorylated DR and spacer region. (**G**) Real-time fluorescence detection curves showing the DR-3′PO_4-assisted CRISPR-Cas12a detection system using varying ALP concentrations. (**H**) Quantitative relationship, linear fitting, and detection limit of fluorescence values versus ALP concentration in the detection system. (**I**) Comparative bar chart of the currently developed DR-3′PO_4-assisted CRISPR-Cas12a system and the clinical PNPP method for ALP detection in 23 human serum samples. Notes: ns, $P > 0.05$, $^{****}P < 0.0001$. Error bars are mean ± SD ($n = 3$).

Downloaded from https://academic.oup.com/nar/article/53/3/gkaf040/7990341 by guest on 10 February 2025

1.22×10^5 M^{-1} S^{-1}, with both exhibiting effective cleavage activity. In contrast, when DR underwent 3′ phosphorylation, there was a substantial drop in catalytic efficiency to 1.57×10^4 M^{-1} S^{-1}, indicating a marked reduction in cleavage activity. Following incubation with ALP, catalytic efficiency rebounded to 1.01×10^5 M^{-1} S^{-1}, reactivating the original cleavage function. This quantitative analysis further substantiates that 3′ phosphorylation of the DR significantly impairs the cleavage function of LbCas12a (Fig. 2D and E; Supplementary Fig. S2).

To explore the molecular mechanisms underlying LbCas12a activity suppression by DR 3′ phosphorylation, we conducted molecular docking simulations. Using LbCas12 as the receptor, we assessed the binding affinities of full-length crRNA, the split form of crRNA (DR + Spacer), and the split form with the 3′ phosphorylated ligands. We utilized available PDB files [51] or predictions from AlphaFold 3 [52], with calculations performed via the HDOCK server [53], followed by visualization using PyMOL. Our results indicated that the split crRNA (DR + Spacer) could bind to LbCas12a efficiently, similar to the full-length crRNA. Conversely, the 3′ phosphorylated DR appeared to interact with other regions of the protein (Fig. 2F). Further analysis of the electrostatic and hydrogen bonding interactions between the 3′ phosphate of DR-3′PO_4 with LbCas12a revealed a tendency for this modification to be attracted to regions with dense positive charges (the PI region), specifically forming multiple hydrogen bonds with ARG-691 and ASN-590 (Fig. 2F and Supplementary Fig. S3). This suggests that the phosphorylation at the 3′ end may alter the classic binding structure of the DR to the protein, thereby inhibiting the normal function of LbCas12a (Fig. 2F and Supplementary Fig. S3).

Subsequently, leveraging the reversible inhibition and restoration capabilities provided by the 3′ phosphorylation modifications, we developed a DR-3′PO_4-assisted CRISPR-Cas12a system for the detection of ALP. ALP is a widely recognized biomarker present in the human body, with blood tests measuring ALP levels as indicators of liver and bone health. Normal serum ALP ranges from 20 to 140 U/L, and elevated levels may signal liver or certain bone diseases [54, 55].

We first validated our engineered CRISPR-Cas12a system using commercially available Calf intestinal ALP. Our results demonstrated that as the concentration of Calf intestinal ALP increased, LbCas12a *trans*-cleavage activity enhanced progressively, exhibiting an excellent detection range with a limit of detection as low as 0.26 U/L (Supplementary Fig. S4). Furthermore, we confirmed that our method maintained impressive detection performance in human serum samples, achieving a limit of detection as low as 0.34 U/L (Fig. 2G and H). We then collected 23 clinical serum samples and compared our findings with the PNPP method, a gold-standard strategy for ALP detection that employs PNPP as a chromogenic substrate [55, 56]. Upon hydrolysis, PNPP produces para-nitrophenol, resulting in a vibrant yellow solution under alkaline conditions, which can be accurately quantified using a spectrophotometer at 405 nm [56]. Our method demonstrated a high degree of concordance with established PNPP results, along with a lower detection limit (Fig. 2H and I; Supplementary Figs S5 and S6). This underscores the broad potential for clinical applications derived from our study on the 3′ terminal phosphorylation of the DR.

Programmable and universal detection platform for rapid protein detection using DR 3′ end phosphorylation enhanced CRISPR-Cas12a system

In clinical diagnostics, while a limited number of biomarkers are nucleic acids, a vast majority pertain to proteins, including antibodies, antigens, and various life-related enzymes [1, 10, 44]. Given the comparable performance of the DR 3′ end phosphorylation modification to the gold standard in ALP detection (Fig. 2G–I), we set out to develop a versatile, programmable detection platform that extends to the rapid detection of any protein. As illustrated in Fig. 3A, we modified the bottom of a microtiter plate with a protein capture agent, termed protein capture agent 1, which selectively enriches relevant proteins from serum samples. Following incubation with human serum samples, the target protein of interest is captured by protein capture agent 1. Residual serum is then washed away, and we incubate with ALP-linked protein capture agent 2, which specifically binds to the target protein, followed by elution. Subsequently, the DR 3′ end phosphorylation enhanced CRISPR-Cas12a system is introduced, facilitating the cleavage of the 3′ end phosphate by ALP, thereby restoring LbCas12a activity. The reactivated enzyme initiates *trans*-cleavage activity, releasing a fluorescent signal. This signal is read using appropriate fluorescence detection equipment to quantify the concentration of the target protein (Fig. 3A).

To validate the feasibility of our design, we selected commercially available mouse immunoglobulin G (IgG) for testing. Initially, we loaded the microtiter plate with Protein G, which is capable of selectively capturing mouse IgG [57]. We then diluted the mouse IgG standard into various concentrations (0–2500 ng/ml) and conducted incubation for system verification. Following this, ALP-labeled goat anti-mouse IgG was introduced and incubated. After elution, we incorporated the CRISPR-Cas12a reaction system, resulting in distinct real-time fluorescence curves (Fig. 3B). We observed a robust linear relationship between fluorescence values and concentrations within the range of 19.5–625 ng/ml, achieving a detection limit as low as 0.29 ng (1.45 ng/ml) (Fig. 3C and Supplementary Fig. S7A). Comparative studies with the gold standard PNPP method demonstrated similar detection performance (Fig. 3B and C; Supplementary Fig. S7).

Encouraged by these successful experiments, we aimed to establish a point-of-care testing (POCT) detection system for visualizing protein concentrations without relying on large instrumentation. We replaced the F-Q in the original system with FAM-Biotin (Supplementary Table S1) and employed lateral flow assay technology on paper test strips [58]. In the absence of the target protein, LbCas12a activity remains inhibited, allowing FAM-Biotin to remain intact. During the chromatography process, FAM-Biotin binds to gold nanoparticles, which capture the biotin moiety at line C, producing a visible signal. In contrast, when target antibody proteins are present, LbCas12a's *trans*-cleavage activity is activated, resulting in the cleavage of FAM-Biotin. The fragments of FAM that are no longer biotinylated evade capture at line C and bind to anti-FAM antibodies at line T (Supplementary Scheme S2). Images of the test strip, captured using a smartphone, reveal that with increasing concentrations of mouse IgG, the signal intensity at line T increases while that at line C decreases, effectively detecting down to 19.6 ng (98 ng/ml) without the use of large detection instruments (Fig. 3D and E).

Downloaded from https://academic.oup.com/nar/article/53/3/gkaf040/7990341 by guest on 10 February 2025

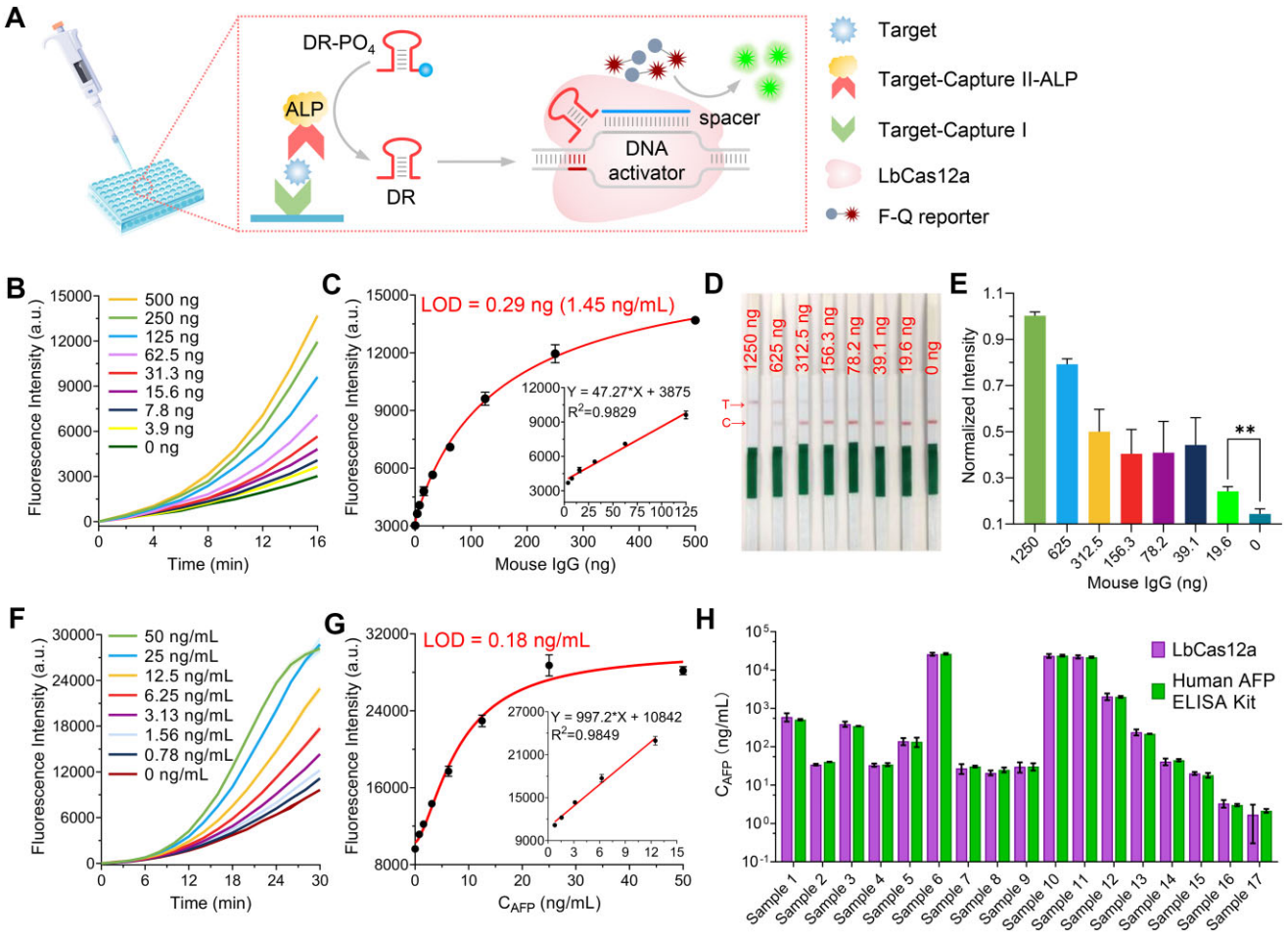


Figure 3. Extending the DR-3′PO_4-assisted CRISPR-Cas12a system to detect any protein. (**A**) Schematic diagram of the universal design for detecting any protein with the DR-3′PO_4-assisted CRISPR-Cas12a system. (**B**) Real-time fluorescence images for different concentrations of mouse IgG using the system. (**C**) Quantitative plot, linear fitting, and detection limit of fluorescence values versus mouse IgG concentration. (**D**) Mobile phone captured images showing paper test strip coloration for varying mouse IgG concentrations. T stands for test, and C stands for control. (**E**) ImageJ software quantitative analysis of color development on IgG paper test strips. (**F**) Real-time fluorescence images for different concentrations of AFP using the system. (**G**) Quantitative plot, linear fitting, and detection limit of fluorescence values versus AFP concentration. (**H**) Comparative bar chart of AFP detection in clinical human serum samples ($n = 17$) using this system against the commercial Human AFP ELISA Kit. Notes: $^{**}P < 0.01$. Error bars are mean ± SD ($n = 3$).

Additionally, we were motivated to investigate the detection of AFP in clinical samples. AFP is a glycoprotein produced and secreted by the liver, yolk sac, and gastrointestinal tract, commonly used to screen for chromosomal abnormalities in fetuses, as well as a significant tumor marker for hepatocellular carcinoma and yolk sac tumors. In normal adults, low levels of AFP can be detected in serum, generally below 10 ng/ml. However, under certain pathological conditions, AFP levels can significantly rise, reaching up to 400 ng/ml, marking its clinical relevance [59–61].

To initiate this investigation, we utilized a microtiter plate pre-coated with antibodies specific to human AFP. Standard samples or clinical human serum samples were introduced into the designated wells, followed by the addition of a biotin-conjugated antibody specific to AFP. Subsequently, avidin conjugated to ALP was added to each well and allowed to incubate. Finally, we introduced the DR 3′ end phosphorylation-enhanced CRISPR-Cas12a system and performed fluorescence detection. Our assay demonstrated a detection limit as low as 0.18 ng/ml, with a linear range of 0.78–12.5 ng/ml (Fig. 3F and G), surpassing the performance of commercially available human AFP ELISA kit with a detection limit of 0.41 ng/ml (Supplementary Fig. S8). We further analyzed and detected AFP levels in 17 human serum samples, comparing the results with the commercial Kit, yielding highly consistent findings (Figs 3H and Supplementary Fig. S9). These results further underscore the universality and applicability of our methodology, suggesting its potential for widespread implementation in clinical diagnostics.

Systematic study and clinical applications of DR-DNA and DR-PC-DNA enhanced CRISPR-Cas12a systems

The critical role of the DR 3′ end in maintaining the activity of LbCas12a has prompted us to enhance its application by adding more modifications such as a DNA sequence at the DR 3′ end (DR-DNA, Supplementary Table S1). The employment of matching different spacer regions, such as EBV, HCV, or MPXV, revealed that DR-DNA effectively impeded the *cis*- and *trans*-cleavage activities of LbCas12a against a range of targets (Fig. 4A and Supplementary Fig. S10). Subsequently,

Downloaded from https://academic.oup.com/nar/article/53/3/gkaf040/7990341 by guest on 10 February 2025

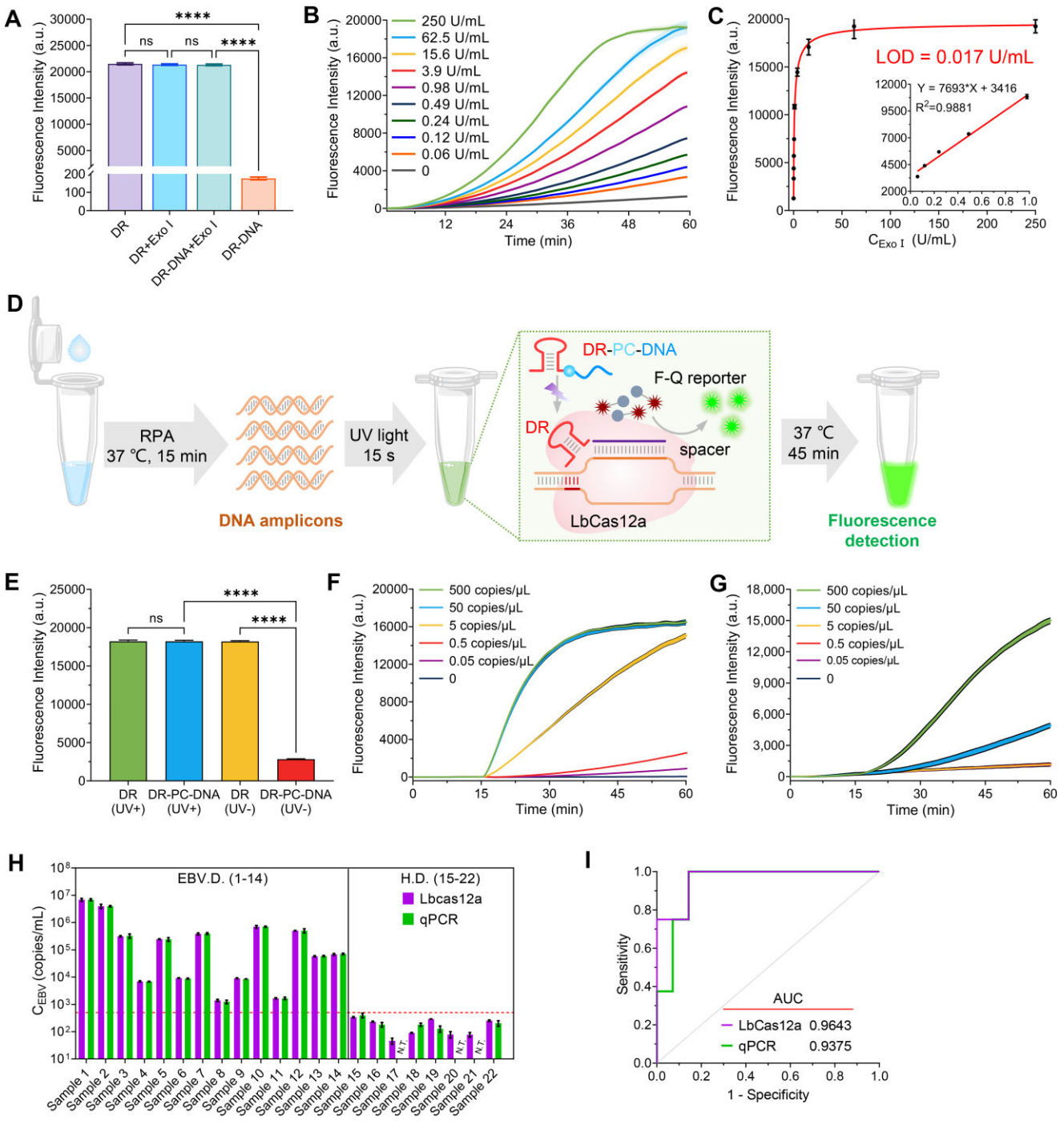


Figure 4. Inhibition and reactivation of LbCas12a through DR-DNA and DR-PC-DNA, along with RPA-CRISPR-Cas12a one-pot detection for clinical trace nucleic acids. (**A**) Quantitative analysis of LbCas12a's *trans*-cleavage activity with classical DR or DR-DNA in the presence and absence of Exo I. (**B**) Real-time quantitative detection of various Exo I concentrations using the DR-DNA-assisted CRISPR-Cas12a system. (**C**) Quantitative relationship, linear fitting, and detection limit of fluorescence values versus Exo I concentration. (**D**) One-pot detection for trace nucleic acids using the RPA-DR-PC-DNA CRISPR-Cas12a system. Initial inhibition of LbCas12a activity is relieved post-UV exposure, enabling the LbCas12a's *trans*-cleavage of the single-stranded F-Q reporter. (**E**) Quantitative fluorescence analysis of LbCas12a's *trans*-cleavage activity with classical DR or DR-PC-DNA under UV and non-UV conditions. (**F**) Real-time fluorescence curve for low-concentration nucleic acid detection using the currently developed RPA-DR-PC-DNA CRISPR-Cas12a one-pot method, measurable down to 0.05 copies/μl. (**G**) Real-time fluorescence curve for low-concentration nucleic acid detection using a classical RPA-crRNA CRISPR-Cas12a one-pot method, measurable down to 50 copies/μl. (**H**) Comparative bar chart of 14 clinical EBV-infected patients and eight healthy donors using the one-pot method against qPCR as the clinical gold standard. The cutoff for EBV load was set at 500 copies/ml. (**I**) Receiver operating characteristic (ROC) curves and area under the curve (AUC) analysis for EBV infection diagnosis, comparing the currently developed RPA-DR-PC-DNA CRISPR-Cas12a one-pot method and a conventional qPCR method. Notes: ns, $P > 0.05$, $^{****}P < 0.0001$. Error bars are mean ± SD ($n = 3$).

Downloaded from https://academic.oup.com/nar/article/53/3/gkaf040/7990341 by guest on 10 February 2025

the DR-DNA was incubated with Exo I to remove the DNA moiety at the DR 3′ end (Supplementary Fig. S11), resulting in the restoration of LbCas12a's cleavage activity (Fig. 4A and Supplementary Fig. S10). Furthermore, by diluting different concentrations of Exo I, we discovered that CRISPR-Cas12a assisted by DR-DNA could effectively detect Exo I, displaying a linear range of 0.06–0.98 U/ml with a detection limit as low as 0.017 U/ml (Fig. 4B and C). This finding holds promise for future applications in Exo I-mediated gene circuits and DNA nanotechnology [62].

Building on this foundation, we inserted a light-sensitive PC linker [35] between the DR and DNA moiety, resulting in the formation of DR-PC-DNA (Table, S1). We confirmed that DR-PC-DNA similarly inhibits the functionality of LbCas12a (Fig. 4E and Supplementary Fig. S12). Notably, after exposure to ultraviolet light for 15 s, the DR-PC-DNA is cleaved (Supplementary Fig. S12), restoring the function of DR and consequently reviving the *cis*- and *trans*-cleavage activities of LbCas12a (Fig. 4E and Supplementary Fig. S13). Encouraged by these results, we designed a universal light-controlled RPA-CRISPR-Cas12a one-pot assay aimed at detecting clinically relevant nucleic acid targets at extremely low concentrations (Fig. 4D).

Traditional RPA-Cas12a one-pot assays face challenges due to the inherent incompatibility between Cas12a and RPA, particularly when detecting very low abundant nucleic acids. Specifically, in scenarios where nucleic acid targets are present at minimal levels, Cas12a can deplete the available templates through rapid *cis*-cleavage before RPA amplification can occur, ultimately hindering the detection process [33, 35]. Recent studies have focused on chemically modifying the crRNA or its complementary strand to temporarily suppress Cas12a activity, allowing for activation post-RPA completion through light control [33, 35, 63]. This approach effectively separates the RPA amplification and CRISPR reaction in terms of timing, addressing compatibility issues in low-concentration nucleic acid templates. Nevertheless, a more general strategy that does not necessitate chemical modification with each application is imperative for clinical implementation.

Given our findings regarding the significance of modifications at the DR 3′ critical site, we have developed a more general and cost-effective light-controlled one-pot method that requires only a single modification at the DR itself (Fig. 4D). This system can accommodate various nucleic acid targets by matching different Spacer. Our detection capability reaches concentrations as low as 0.05 copies/μl, markedly <50 copies/μl threshold established by traditional RPA-CRISPR-Cas12a one-pot methods (Fig. 4F and G; Supplementary Fig. S14).

As a proof of concept for clinical applications, we employed the DR-PC-DNA-assisted CRISPR-Cas12a system to detect EBV in serum samples (Fig. 4H and I; Supplementary Fig. S15). We collected serum samples from 14 EBV-infected patients and 8 healthy donors, extracting total DNA from 200 μl of serum. We then conducted parallel testing using both the DR-PC-DNA-assisted CRISPR-Cas12a method and conventional qPCR (Supplementary Fig. S16). As anticipated, EBV-infected patients exhibited markedly higher EBV copy numbers compared to healthy donors (Fig. 4H and I). Importantly, our method demonstrated remarkable consistency with the classic qPCR findings while achieving a lower detection limit, validating the high efficacy of our approach (Fig. 4H and I; Supplementary Fig. S17). ROC curve analysis [64] quantitatively evaluated the diagnostic performance of the CRISPR-Cas12a system for detecting viral nucleic acids in serum. The DR-PC-DNA-assisted CRISPR-Cas12a detection yielded a satisfactory AUC value of 0.9643, comparable to that of qPCR (0.9375), further affirming the robustness of our method in viral infection diagnostics (Fig. 4I).

Introduction of DNA modifications at the 3′ end of DR and their application in the detection of DNA glycosylases

Subsequently, we explored the effectiveness of inhibiting LbCas12a activity by introducing different DNA modifications at the DR 3′ end. We further investigated whether the treatment of DNA glycosylases corresponding to these DNA modifications could effectively restore activity. The function of DNA glycosylases is to maintain genome integrity by recognizing and repairing damaged DNA [65]. The relative abundance of these enzymes is considered to be a diagnostic biomarker for various diseases, which highlights the necessity for accurate and timely detection technologies [66, 67]. In our design, we inserted a DNA modification into the middle of a random sequence of DNA following DR, followed by the addition of a segment of RNA (Fig. 5A). And the DNA exonucleases are unable to digest the DR-DNA-RNA structure (Fig. 5A and Supplementary Table S1). Subsequently, dual-function DNA glycosylases like OGG1, capable of both base excision repair and AP-lyase activities, can recognize and cleave the DNA modification (e.g. 8OG corresponding to OGG1) to form an AP site [67]. Subsequently, under the action of its AP-lyase activity, beta elimination occurs, breaking the bond to generate 3′-phospho-α, β-unsaturated aldehyde. This is followed by delta elimination and the cleavage of the remaining residual DNA by the exonucleases, restoring LbCas12a activity. And for single-function DNA glycosylases like UDG (possessing only base excision activity), spermine in the reaction system further reacts with the generated AP site to promote beta elimination and the eventual breakage of the bond [68]. The DNA modification in this design is programmable and can be replaced, thus facilitating the recognition and response of different DNA glycosylases via the introduction of their corresponding DNA modifications (Fig. 5A).

To validate our experiments, we designed and synthesized DR-dU-RNA containing dU, DR-8OG-RNA containing 8OG, and DR-THF-RNA containing a mimic AP site (corresponding to DNA glycosylases UDG, OGG1, and APE1, respectively, Supplementary Table S1). Using PAGE, we demonstrated that exonucleases could not digest the DR-DNA modification-RNA structure. However, following treatment with the corresponding DNA glycosylases, the structure could be further digested by exonucleases, reverting back to DR structure (Supplementary Fig. S18). Subsequently, we tested the effect of DR-dU-RNA on the *trans*-cleavage activity of LbCas12a in systems with and without UDG. We found that compared to the classic DR, DR-dU-RNA similarly effectively inhibited the *trans*-cleavage activity of LbCas12a (Supplementary Fig. S19A).

After incubation with UDG and subsequent exonuclease treatment, the *trans*-cleavage activity of LbCas12a was restored, with a recovery rate of up to 87.4% (Supplementary Fig. S19B). Following this, we diluted various UDG standards and detected different UDG levels in the system, observing that with increasing UDG content, the fluorescence intensity

Downloaded from https://academic.oup.com/nar/article/53/3/gkaf040/7990341 by guest on 10 February 2025

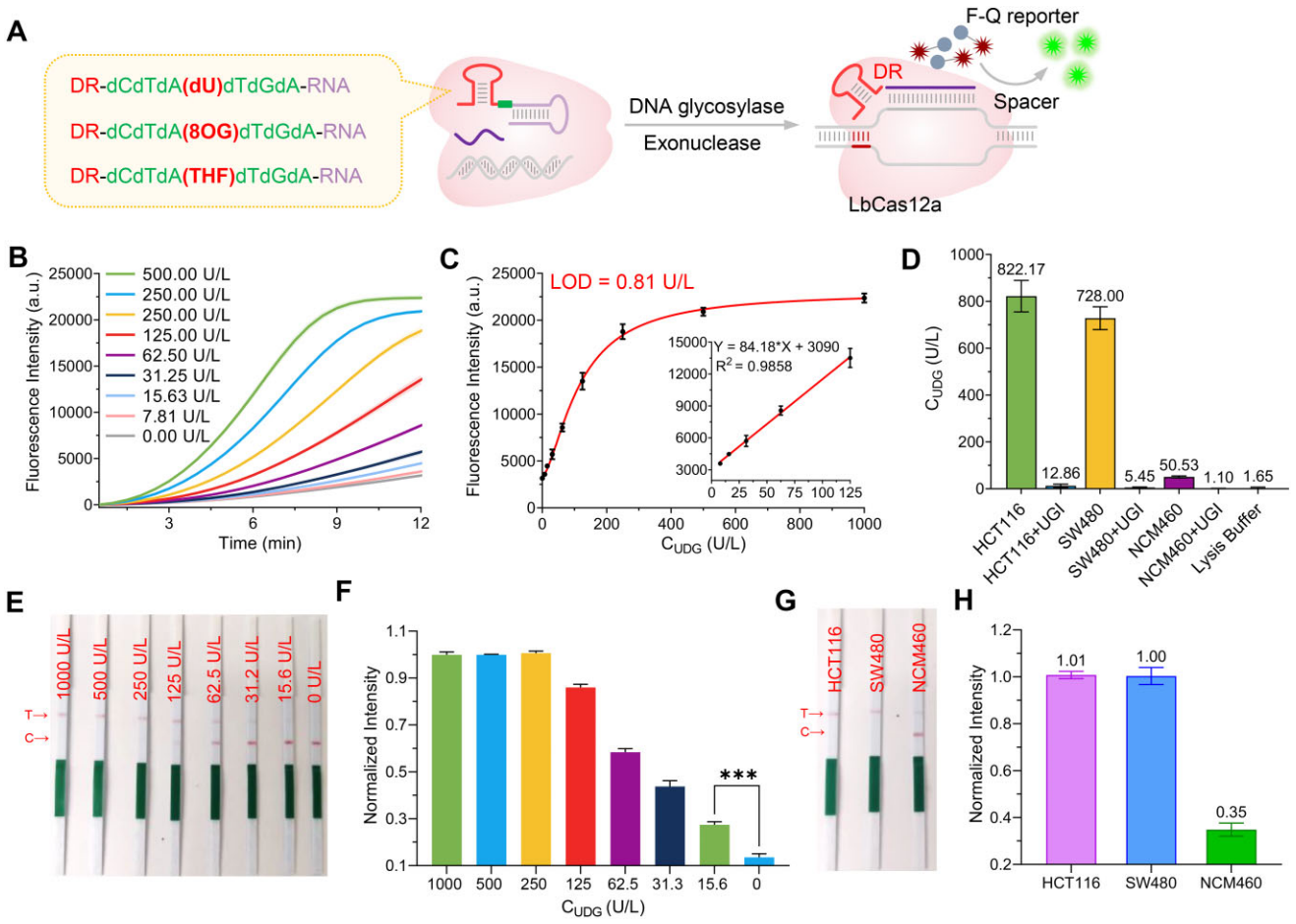


Figure 5. Programmable detection of various DNA glycosylases by introducing DNA modifications at the DR 3′ end. (**A**) Schematic illustrating detection mechanisms for DNA glycosylases using dU, 8OG, and THF modified at the DR 3′ end. (**B**) Real-time quantitative fluorescence detection for varying UDG concentrations using the DR-dU-RNA-assisted CRISPR-Cas12a system. (**C**) Quantitative relationship, linear fitting, and detection limit of fluorescence values versus UDG concentration. (**D**) Quantitative detection of nuclear extracts from HCT116, SW480, and NCM460 cells, with and without UGI (UDG inhibitor), using the system. (**E**) Mobile phone captured images of paper test strip coloration for different UDG concentrations. T stands for test and C stands for control. (**F**) Quantitative analysis via ImageJ of color development on UDG paper test strips. Mobile phone captured detection results (**G**) and ImageJ analysis (**H**) for nuclear protein extracts from the above-mentioned cell lines using the DR-dU-RNA paper test strip system. Notes: ns, $P > 0.05$, $^{***}P < 0.001$. Error bars are mean ± SD ($n = 3$).

gradually enhanced within a range of 7.81–125 U/L, displaying excellent linearity with a detection limit reaching 0.81 U/L (Fig. 5B and C). Next, we extracted nuclear proteins from colon cancer cell lines HCT116, SW480, and colon non-cancerous cell lines NCM460, and verified them using our system. We found that the UDG content in colon cancer cells was significantly higher than in non-cancerous cells, aligning with existing literature [69] (Fig. 5D). Furthermore, upon the addition of UGI (an UDG inhibitor) to the nuclear protein extracts, the fluorescence signal in the system diminished, further confirming the high selectivity and efficacy of our detection method (Fig. 5D). Subsequently, to test if this method could facilitate POCT, we replaced the original F-Q reporter with FAM-Biotin and utilized paper strips for testing. Diluting UDG standards, we observed that as UDG content increased, the signal at the C line weakened while the T line intensified. Through quantitative analysis using ImageJ, we detected UDG content as low as 15.6 U/L (Fig. 5E and F). Furthermore, we applied the same paper strip method to detect UDG content in cells, corroborating the results obtained through fluorescence detection, showing that UDG content in colon cancer cell lines was indeed higher than in non-cancerous cells (Fig. 5G and H).

To demonstrate the programmability of this method, we also tested DR-8OG-RNA and DR-THF-RNA, which effectively inhibited LbCas12a activity and restored the activity under the corresponding actions of OGG1 or APE1. Additionally, we tested LbCas12a assisted by DR-8OG-RNA for OGG1 detection, yielding a linear range of 125–2000 U/ml with a detection limit as low as 26.66 U/ml. Similarly, DR-THF-RNA could be used for APE1 detection, displaying a linear range of 156.3–5000 U/ml with a detection limit as low as 39.33 U/ml (Supplementary Figs S20 and S21). By demonstrating the method's programmability, we have shown its potential for detecting enzymes corresponding to various DNA modifications, presenting significant expansion possibilities.

Discussion

In this study, we have elucidated a critical regulatory mechanism of LbCas12a by demonstrating that modifications and de-modifications on the 3′ end of its DR can suppress and re-

Downloaded from https://academic.oup.com/nar/article/53/3/gkaf040/7990341 by guest on 10 February 2025

store both its *cis*- and *trans*-cleavage activities. This discovery not only enhances our understanding of LbCas12a functionality but also has significant implications for its application in diagnostic settings. To investigate whether the 3′ phosphate modification of DR and ALP treatment exert similar effects on other Cas12a variants, we conducted comparative analyses with ErCas12a, ArCas12a, and FnCas12a, in addition to LbCas12a. Our experimental results demonstrated that the 3′ phosphate modification consistently inhibited the activity across these diverse Cas12a variants, and subsequent ALP-mediated dephosphorylation effectively restored their functionality (Supplementary Fig. S22). These findings suggest that the regulatory mechanism identified in LbCas12a may represent a conserved feature among Cas12a family members, thereby significantly expanding the potential applications and implications of our discovery.

Our findings were applied to the clinical detection of ALP, with results comparable to those obtained from the gold standard PNPP method. We further expanded the application of this approach to develop a platform for the detection of various proteins and successfully identified AFP in clinical serum samples, achieving performance levels consistent with commercial ELISA kits. Current commercial detection of AFP predominantly relies on ELISA-based chemiluminescence methods. In our study, we have developed a detection platform that utilizes the fluorescence signal generated by LbCas12a *trans*-cleavage activity. Notably, while maintaining comparable detection limits, our LbCas12a-based approach offers significant advantages for POCT applications, particularly in lateral flow assay formats. This methodological advancement represents a paradigm shift in AFP detection technology, providing enhanced practicality for clinical diagnostics.

Additionally, our exploration of inserting DNA into the 3′ end of the DR confirmed its ability to inhibit LbCas12a activity, which could be restored through the action of exonucleases. We developed a universal light-controllable RPA-CRISPR-Cas12a one-pot assay by incorporating a PC linker between DR and DNA moiety, enabling a straightforward and adaptable method for the detection of different targets. The assay demonstrated efficacy in identifying EBV in human serum, yielding results on par with the gold standard qPCR. Our DR-PC-DNA-assisted LbCas12a detection system demonstrates several distinct advantages over conventional qPCR-based nucleic acid detection methods: (i) a simplified operational workflow; (ii) isothermal detection at 37°C; (iii) minimal instrumentation requirements; (iv) compatibility with lateral flow strip-based visual detection for rapid and convenient on-site applications; and (v) significantly enhanced detection sensitivity, enabling the identification of target nucleic acids at lower concentrations. While these advantages are significant, we acknowledge certain limitations in the current system. Specifically, (i) the current cost of LbCas12a protein remains relatively high compared to Taq polymerase in qPCR, primarily due to its limited commercial availability. However, we anticipate cost reductions with increased market adoption. (ii) The photo-controlled initiation of RPA-CRISPR-Cas12a one-pot assays requires light-sensitive nucleic acids (e.g. DR-PC-DNA), which necessitate light-protected storage to maintain stability and efficacy. Although our experiments have shown that DR-PC DNA is sufficiently robust under laboratory light without additional light protection during operation (Supplementary Fig. S23), proper storage protocols remain essential. (iii) While our method exhibits superior sensitivity compared to qPCR, the selection of appropriate cut-off values becomes particularly critical in clinical sample detection. This aspect warrants thorough investigation and careful consideration during clinical implementation.

Moreover, we investigated the effects of introducing DNA modifications following the DR. Our results showed that the DR-DNA modification-RNA structure could also inhibit LbCas12a activity, which could be reactivated by corresponding DNA glycosylases. This programmability allows for flexible detection of various DNA glycosylases via different modification introduction. Our finding builds upon the previously established Cas12a split crRNA strategy [23–25, 70]. Inspired by Chen *et al.*'s discovery that miRNAs can functionally replace the Spacer in split crRNA systems [25], we sought to expand the scope and potential applications of our research. Specifically, we investigated the regulation of LbCas12a *trans*-cleavage activity by DR-3′PO_4 and ALP under the guidance of four distinct miRNAs: miR-92a, miR-429, miR-31, and miR-17. Our experimental results (Supplementary Fig. S24) reveal that these miRNAs can effectively guide LbCas12a *trans*-cleavage activity when paired with DR in the presence of their corresponding DNA targets (Supplementary Table S1). However, we observed that 3′ phosphorylation of DR completely inhibits the miRNA-mediated guidance function. Notably, this inhibition is reversible through ALP-mediated removal of the 3′ phosphate group, which restores the miRNA's ability to activate LbCas12a. These findings significantly broaden the scope of potential applications for our discovery, revealing that the DR 3′ end modification and de-modification system is capable of regulating miRNA-guided Cas12a activity.

In conclusion, our investigations into the 3′ end modifications of the DR have not only provided insight into the regulatory mechanisms governing LbCas12a activity but have also significantly expanded its potential for detecting clinic targets. This work lays the basis for further diagnostic applications and highlights the versatility of LbCas12a in new biomedical contexts.

Acknowledgements

Author contributions: W. Z., Y. Z., and J. W. contributed equally to this work. C. L., W. Z., and J. W. were responsible for conceptualization, methodology, writing the original draft, reviewing and editing the manuscript, and supervision. W. Z., Y. Z., and J. W. performed experimental work, conducted data curation, formal analysis, investigation, and visualization. G.Z. and Q.C. contributed to data curation, formal analysis, software implementation, and resource management. All authors reviewed and approved the final manuscript.

Supplementary data

Supplementary data is available at NAR online.

Conflict of interest

None declared.

Funding

This work was supported by National Natural Science Foundation of China (22307150), Shenzhen Medical Research Fund (A2303012), Guangdong Basic and Applied Basic Research Foundation (2024A1515012319), Shenzhen Sci-

Downloaded from https://academic.oup.com/nar/article/53/3/gkaf040/7990341 by guest on 10 February 2025

ence and Technology Program (JCYJ20230807110315032, JCYJ20240813150427036).

Data availability

The data supporting the findings of this study are available in the Supplementary Material of this article, which includes detailed chemical and material information, nucleic acid sequences (Supplementary Table S1), an abbreviation reference table for this work (Supplementary Table S2), and supplementary figures.

References

1. Tang Y, Gao L, Feng W *et al.* The CRISPR–Cas toolbox for analytical and diagnostic assay development. *Chem Soc Rev* 2021;**50**:11844–69. https://doi.org/10.1039/D1CS00098E
2. Makarova KS, Wolf YI, Alkhnbashi OS *et al.* An updated evolutionary classification of CRISPR-Cas systems. *Nat Rev Micro* 2015;**13**:722–36. https://doi.org/10.1038/nrmicro3569
3. Pickar-Oliver A, Gersbach CA. The next generation of CRISPR–Cas technologies and applications. *Nat Rev Mol Cell Biol* 2019;**20**:490–507. https://doi.org/10.1038/s41580-019-0131-5
4. Chen JS, Ma EB, Harrington LB *et al.* CRISPR-Cas12a target binding unleashes indiscriminate single-stranded DNase activity. *Science* 2018;**360**:436–39. https://doi.org/10.1126/science.aar6245
5. Li SY, Cheng QX, Liu JK *et al.* CRISPR-Cas12a has both *cis*- and *trans*-cleavage activities on single-stranded DNA. *Cell Res* 2018;**28**:491–93. https://doi.org/10.1038/s41422-018-0022-x
6. Chen J, Chen Y, Huang L *et al. Trans*-nuclease activity of Cas9 activated by DNA or RNA target binding. *Nat Biotechnol* 2024. https://doi.org/10.1038/s41587-024-02255-7
7. Lyu Y, He S, Li J *et al.* A photolabile semiconducting polymer nanotransducer for near-infrared regulation of CRISPR/Cas9 gene editing. *Angew Chem Int Ed Engl* 2019;**58**:18197–18201. https://doi.org/10.1002/anie.201909264
8. Mahas A, Stewart Jr CN, Mahfouz MM. Harnessing CRISPR/Cas systems for programmable transcriptional and post-transcriptional regulation. *Biotechnol Adv* 2018;**36**:295–310. https://doi.org/10.1016/j.biotechadv.2017.11.008
9. McCarty NS, Graham AE, Studená L *et al.* Multiplexed CRISPR technologies for gene editing and transcriptional regulation. *Nat Commun* 2020;**11**:1281. https://doi.org/10.1038/s41467-020-15053-x
10. Kaminski MM, Abudayyeh OO, Gootenberg JS *et al.* CRISPR-based diagnostics. *Nat Biomed Eng* 2021;**5**:643–656. https://doi.org/10.1038/s41551-021-00760-7
11. Yang Y, Xu J, Ge S *et al.* CRISPR/Cas: advances, limitations, and applications for precision cancer research. *Front Med* 2021;**8**:649896. https://doi.org/10.3389/fmed.2021.649896
12. Polstein LR, Gersbach CA. A light-inducible CRISPR-Cas9 system for control of endogenous gene activation. *Nat Chem Biol* 2015;**11**:198–200. https://doi.org/10.1038/nchembio.1753
13. Nihongaki Y, Yamamoto S, Kawano F *et al.* CRISPR-Cas9-based photoactivatable transcription system. *Chem Biol* 2015;**22**:169–74. https://doi.org/10.1016/j.chembiol.2014.12.011
14. Wang X, Dong K, Kong D *et al.* A far-red light–inducible CRISPR-Cas12a platform for remote-controlled genome editing and gene activation. *Sci Adv* 2021;**7**:eabh2358. https://doi.org/10.1126/sciadv.abh2358
15. Nguyen LT, Rananaware SR, Yang LG *et al.* Engineering highly thermostable Cas12b via *de novo* structural analyses for one-pot detection of nucleic acids. *Cell Rep Med* 2023;**4**:101037. https://doi.org/10.1016/j.xcrm.2023.101037
16. Slaymaker IM, Gao L, Zetsche B *et al.* Rationally engineered Cas9 nucleases with improved specificity. *Science* 2016;**351**:84–8. https://doi.org/10.1126/science.aad5227
17. Schmid-Burgk JL, Gao L, Li D *et al.* Highly parallel profiling of Cas9 variant specificity. *Mol Cell* 2020;**78**:794–800.e8. https://doi.org/10.1016/j.molcel.2020.02.023
18. Teng F, Guo L, Cui T *et al.* CDetection: CRISPR-Cas12b-based DNA detection with sub-attomolar sensitivity and single-base specificity. *Genome Biol* 2019;**20**:132. https://doi.org/10.1186/s13059-019-1742-z
19. Kim H, Lee W-j, Oh Y *et al.* Enhancement of target specificity of CRISPR–Cas12a by using a chimeric DNA–RNA guide. *Nucleic Acids Res* 2020;**48**:8601–8616. https://doi.org/10.1093/nar/gkaa605
20. Nguyen LT, Smith BM, Jain PK. Enhancement of trans-cleavage activity of Cas12a with engineered crRNA enables amplified nucleic acid detection. *Nat Commun* 2020;**11**:4906.https://doi.org/10.1038/s41467-020-18615-1
21. McMahon MA, Prakash TP, Cleveland DW *et al.* Chemically modified Cpf1-CRISPR RNAs mediate efficient genome editing in mammalian cells. *Mol Ther* 2018;**26**:1228–1240. https://doi.org/10.1016/j.ymthe.2018.02.031
22. Fu Y, Sander JD, Reyon D *et al.* Improving CRISPR-Cas nuclease specificity using truncated guide RNAs. *Nat Biotechnol* 2014;**32**:279–284. https://doi.org/10.1038/nbt.2808
23. Shebanova R, Nikitchina N, Shebanov N *et al.* Efficient target cleavage by Type V Cas12a effectors programmed with split CRISPR RNA. *Nucleic Acids Res* 2022;**50**:1162–1173. https://doi.org/10.1093/nar/gkab1227
24. Moon J, Liu C. Asymmetric CRISPR enabling cascade signal amplification for nucleic acid detection by competitive crRNA. *Nat Commun* 2023;**14**:7504. https://doi.org/10.1038/s41467-023-43389-7
25. Chen Y, Wang X, Zhang J *et al.* Split crRNA with CRISPR-Cas12a enabling highly sensitive and multiplexed detection of RNA and DNA. *Nat Commun* 2024;**15**:8342. https://doi.org/10.1038/s41467-024-52691-x
26. Deng H, Xu H, Wang Y *et al.* G-quadruplex-based CRISPR photoswitch for spatiotemporal control of genomic modulation. *Nucleic Acids Res* 2023;**51**:4064–4077. https://doi.org/10.1093/nar/gkad178
27. Liu X, Cui S, Qi Q *et al.* G-quadruplex-guided RNA engineering to modulate CRISPR-based genomic regulation. *Nucleic Acids Res* 2022;**50**:11387–11400. https://doi.org/10.1093/nar/gkac870
28. Qi Q, Liu X, Fu F *et al.* Utilizing epigenetic modification as a reactive handle to regulate RNA function and CRISPR-based gene regulation. *J Am Chem Soc* 2023;**145**:11678–11689. https://doi.org/10.1021/jacs.3c01864
29. Hu Z, Sun A, Yang J *et al.* Regulation of the CRISPR-Cas12a system by methylation and demethylation of guide RNA. *Chem Sci* 2023;**14**:5945–5955. https://doi.org/10.1039/D3SC00629H
30. Xun G, Zhu Z, Singh N *et al.* Harnessing noncanonical crRNA for highly efficient genome editing. *Nat Commun* 2024;**15**:3823. https://doi.org/10.1038/s41467-024-48012-x
31. Sheng A, Yang J, Tang L *et al.* Hydrazone chemistry-mediated CRISPR/Cas12a system for bacterial analysis. *Nucleic Acids Res* 2022;**50**:10562–10570. https://doi.org/10.1093/nar/gkac809
32. Ling X, Chang L, Chen H *et al.* Improving the efficiency of CRISPR-Cas12a-based genome editing with site-specific covalent Cas12a-crRNA conjugates. *Mol Cell* 2021;**81**:4747–4756.e7. https://doi.org/10.1016/j.molcel.2021.09.021
33. Hu M, Liu R, Qiu Z *et al.* Light-start CRISPR-Cas12a reaction with caged crRNA enables rapid and sensitive nucleic acid detection. *Angew Chem Int Ed Engl* 2023;**62**:e202300663. https://doi.org/10.1002/anie.202300663
34. Fei X, Lei C, Ren W *et al.* Regulating the *trans*-cleavage activity of CRISPR/Cas12a by using an elongation-caged single-stranded DNA activator and the biosensing applications. *Anal Chem* 2023;**95**:12169–12176. https://doi.org/10.1021/acs.analchem.3c02471
35. Hu M, Qiu Z, Bi Z *et al.* Photocontrolled crRNA activation enables robust CRISPR-Cas12a diagnostics. *Proc Natl Acad Sci USA* 2022;**119**:e2202034119. https://doi.org/10.1073/pnas.2202034119

Downloaded from https://academic.oup.com/nar/article/53/3/gkaf040/7990341 by guest on 10 February 2025

36. Liu X, Kang X, Lei C *et al.* Programming the *trans*-cleavage activity of CRISPR-Cas13a by single-strand DNA blocker and its biosensing application. *Anal Chem* 2022;**94**:3987–3996. https://doi.org/10.1021/acs.analchem.1c05124
37. Chen Y, Xu X, Wang J *et al.* Photoactivatable CRISPR/Cas12a strategy for one-pot DETECTR molecular diagnosis. *Anal Chem* 2022;**94**:9724–9731. https://doi.org/10.1021/acs.analchem.2c01193
38. Li B, Zeng C, Li W *et al.* Synthetic oligonucleotides inhibit CRISPR-Cpf1-mediated genome editing. *Cell Rep* 2018;**25**:3262–3272.e3. https://doi.org/10.1016/j.celrep.2018.11.079
39. Li Y, Yang X, Dong Y *et al.* CRISPR–Cas12a detection of DNA glycosylases via DNA modification switching. *Chem Commun* 2024;**60**:12569–12572. https://doi.org/10.1039/D4CC04180A
40. Rossetti M, Merlo R, Bagheri N *et al.* Enhancement of CRISPR/Cas12a *trans*-cleavage activity using hairpin DNA reporters. *Nucleic Acids Res* 2022;**50**:8377–8391. https://doi.org/10.1093/nar/gkac578
41. Li F, Li J, Yang W *et al.* Framework-hotspot enhanced trans cleavage of CRISPR-Cas12a for clinical samples detection. *Angew Chem Int Ed Engl* 2023;**62**:e202305536. https://doi.org/10.1002/anie.202305536
42. Fu X, Shi Y, Peng F *et al.* Exploring the trans-cleavage activity of CRISPR/Cas12a on gold nanoparticles for stable and sensitive biosensing. *Anal Chem* 2021;**93**:4967–4974. https://doi.org/10.1021/acs.analchem.1c00027
43. Yuan A, Sha R, Xie W *et al.* RNA-activated CRISPR/Cas12a nanorobots operating in living cells. *J Am Chem Soc* 2024;**146**:26657–26666. https://doi.org/10.1021/jacs.4c02354
44. Xiong Y, Zhang J, Yang Z *et al.* Functional DNA regulated CRISPR-Cas12a sensors for point-of-care diagnostics of non-nucleic-acid targets. *J Am Chem Soc* 2020;**142**:207–213. https://doi.org/10.1021/jacs.9b09211
45. Deng F, Li Y, Yang B *et al.* Topological barrier to Cas12a activation by circular DNA nanostructures facilitates autocatalysis and transforms DNA/RNA sensing. *Nat Commun* 2024;**15**:1818. https://doi.org/10.1038/s41467-024-46001-8
46. Hu M, Cheng X, Wu T. Modular CRISPR/Cas12a synergistic activation platform for detection and logic operations. *Nucleic Acids Res* 2024;**52**:7384–7396. https://doi.org/10.1093/nar/gkae470
47. Rananaware SR, Vesco EK, Shoemaker GM *et al.* Programmable RNA detection with CRISPR-Cas12a. *Nat Commun* 2023;**14**:5409. https://doi.org/10.1038/s41467-023-41006-1
48. Nguyen GT, Schelling MA, Raju A *et al.* CRISPR-Cas12a exhibits metal-dependent specificity switching. *Nucleic Acids Res* 2024;**52**:9343–9359. https://doi.org/10.1093/nar/gkae613
49. Xu Z, Chen D, Li T *et al.* Microfluidic space coding for multiplexed nucleic acid detection via CRISPR-Cas12a and recombinase polymerase amplification. *Nat Commun* 2022;**13**:6480. https://doi.org/10.1038/s41467-022-34086-y
50. Zhang J, Li Z, Guo C *et al.* Intrinsic RNA targeting triggers indiscriminate DNase activity of CRISPR-Cas12a. *Angew Chem Int Ed Engl* 2024;**63**:e202403123. https://doi.org/10.1002/anie.202403123
51. Zhang H, Li Z, Daczkowski CM *et al.* Structural basis for the inhibition of CRISPR-Cas12a by anti-CRISPR proteins. *Cell Host Microbe* 2019;**25**:815–826.e4. https://doi.org/10.1016/j.chom.2019.05.004
52. Abramson J, Adler J, Dunger J *et al.* Accurate structure prediction of biomolecular interactions with AlphaFold 3. *Nature* 2024;**630**:493–500. https://doi.org/10.1038/s41586-024-07487-w
53. Yan Y, Tao H, He J *et al.* The HDOCK server for integrated protein–protein docking. *Nat Protoc* 2020;**15**:1829–1852. https://doi.org/10.1038/s41596-020-0312-x
54. Wannamethee SG, Sattar N, Papcosta O *et al.* Alkaline phosphatase, serum phosphate, and incident cardiovascular disease and total mortality in older men. *Arterioscler Thromb Vasc Biol* 2013;**33**:1070–76. https://doi.org/10.1161/ATVBAHA.112.300826
55. Sharma U, Pal D, Prasad R. Alkaline phosphatase: an overview. *Ind J Clin Biochem* 2014;**29**:269–78. https://doi.org/10.1007/s12291-013-0408-y
56. Burtis CA, Seibert LE, Baird MA *et al.* Temperature dependence of the absorbance of alkaline solutions of 4-nitrophenyl phosphate–a potential source of error in the measurement of alkaline phosphatase activity. *Clin Chem* 1977;**23**:1541–47. https://doi.org/10.1093/clinchem/23.9.1541
57. Wuhrer M, Stam JC, van de Geijn FE *et al.* Glycosylation profiling of immunoglobulin G (IgG) subclasses from human serum. *Proteomics* 2007;**7**:4070–81. https://doi.org/10.1002/pmic.200700289
58. Mukama O, Wu JH, Li ZY *et al.* An ultrasensitive and specific point-of-care CRISPR/Cas12 based lateral flow biosensor for the rapid detection of nucleic acids. *Biosens Bioelectron* 2020;**159**:112143. https://doi.org/10.1016/j.bios.2020.112143
59. Galle PR, Foerster F, Kudo M *et al.* Biology and significance of alpha-fetoprotein in hepatocellular carcinoma. *Liver Int* 2019;**39**:2214–2229. https://doi.org/10.1111/liv.14223
60. Di Bisceglie AM, Hoofnagle JH. Elevations in serum alpha-fetoprotein levels in patients with chronic hepatitis B. *Cancer* 1989;**64**:2117–20. https://doi.org/10.1002/1097-0142(19891115)64:10%3c2117::AID-CNCR2820641024%3e3.0.CO;2-7
61. Abelev G. Alpha-fetoprotein as a marker of embryo-specific differentiations in normal and tumor tissues. *Transplant Rev* 1974;**20**:3–37.
62. Chen J, Fu S, Zhang C *et al.* DNA logic circuits for cancer theranostics. *Small* 2022;**18**:2108008. https://doi.org/10.1002/smll.202108008
63. Liu P, Lin Y, Zhuo X *et al.* Universal crRNA acylation strategy for robust photo-initiated one-pot CRISPR–Cas12a nucleic acid diagnostics. *Angew Chem Int Ed Engl* 2024;**63**:e202401486. https://doi.org/10.1002/anie.202401486
64. Hanley JA. Receiver operating characteristic (ROC) methodology: the state of the art. *Crit Rev Diagn Imaging* 1989;**29**:307–35.
65. Krokan HE, Standal R, Slupphaug G. DNA glycosylases in the base excision repair of DNA. *Biochem J* 1997;**325**:1–16. https://doi.org/10.1042/bj3250001
66. Li G, Henry SA, Liu H *et al.* A robust photoluminescence screening assay identifies uracil-DNA glycosylase inhibitors against prostate cancer. *Chem Sci* 2020;**11**:1750–60. https://doi.org/10.1039/C9SC05623H
67. Sliwinska A, Kwiatkowski D, Czarny P *et al.* The levels of 7, 8-dihydrodeoxyguanosine (8-oxoG) and 8-oxoguanine DNA glycosylase 1 (OGG1)–A potential diagnostic biomarkers of Alzheimer's disease. *J Neurol Sci* 2016;**368**:155–59. https://doi.org/10.1016/j.jns.2016.07.008
68. Haldar T, Jha JS, Yang Z *et al.* Unexpected complexity in the products arising from NaOH-, heat-, amine-, and glycosylase-induced strand cleavage at an abasic site in DNA. *Chem Res Toxicol* 2022;**35**:218–32. https://doi.org/10.1021/acs.chemrestox.1c00409
69. Zhang Q, Li C-c, Ma F *et al.* Catalytic single-molecule Förster resonance energy transfer biosensor for uracil-DNA glycosylase detection and cellular imaging. *Biosens Bioelectron* 2022;**213**:114447. https://doi.org/10.1016/j.bios.2022.114447
70. Huang W, Wang J, Wang C *et al.* Expanding Cas12a activity control with an RNA G-quadruplex at the 5′ end of CRISPR RNA. *Adv Sci* 2024;2411305. https://doi.org/10.1002/advs.202411305

Received: December 2, 2024. **Revised:** January 13, 2025. **Editorial Decision:** January 14, 2025. **Accepted:** January 16, 2025
© The Author(s) 2025. Published by Oxford University Press on behalf of Nucleic Acids Research.
This is an Open Access article distributed under the terms of the Creative Commons Attribution-NonCommercial License (https://creativecommons.org/licenses/by-nc/4.0/), which permits non-commercial re-use, distribution, and reproduction in any medium, provided the original work is properly cited. For commercial re-use, please contact reprints@oup.com for reprints and translation rights for reprints. All other permissions can be obtained through our RightsLink service via the Permissions link on the article page on our site—for further information please contact journals.permissions@oup.com.

Downloaded from https://academic.oup.com/nar/article/53/3/gkaf040/7990341 by guest on 10 February 2025